PREDICTION OF AN INDUSTRIAL FRAMEWORK FOR SEMICONDUCTOR FABRICATION AND EXPERIMENTAL VALIDATION OF 300 MM WAFER

Da-Woon Jeong[1,2,†], Se-hyun Cha[1], Tae-Hyun Kim[3,4], Wangyu Gwak[4], Yangwook Choi[1], HyeongGeun An[1], Eun-Ho Lee[3,4,5]

[1]Memory CVD Technology Team, Samsung Electronics,suwon-si, Gyeonggi-do ,16677, Republic of Korea
[2]Department of Semiconductor and Display engineering, Sungkyunkwan university, suwon, Gyeonggi-do,16419, Republic of Korea
[3]School of Mechanical Engineering, Sungkyunkwan university, Suwon, Gyeonggi-do,16419, Republic of korea
[4]Department of Smart Fab. Technology, Sungkyunkwan university, Suwon, Gyeonggi-do,16419, Republic of Korea
[5]Department of Smart Robotics, Sungkyunkwan university, Suwon, Gyeonggi-do,16419, Republic of Korea
Presentor : dw12.jeong@g.skku.edu[†]
Corresponding author : e.h.lee@skku.edu
Ph;82-10-3120-3631; Fax; 82 31 299 4909

Abstract

In contemporary memory semiconductor manufacturing, optimizing recipes has emerged as a crucial strategy to align with RE100 commitments, bolster ESG ratings, and substantially reduce operational costs. The current landscape demands the development of low-power manufacturing recipes that not only curtail energy consumption but also trim operational expenses, thereby augmenting overall profitability. This underscores the critical necessity for meticulous recipe optimization to ensure both sustainability and economic viability in the industry.

In response to these challenges, there is an urgent need for a predictive framework capable of accurately forecasting optimal recipes. Such a framework is essential for facilitating the industry's adaptation to dynamic technological environments and stringent environmental standards. By enabling proactive adjustments to manufacturing processes, this predictive approach ensures companies remain competitive while advancing comprehensive sustainability objectives.

To address these needs, this work introduces a predictive framework specifically tailored to forecast recipe steps for plasma processes in semiconductor manufacturing. The framework's efficacy was empirically validated using measurements from 300mm wafers in semiconductor mass production equipment. Plasma behavior was meticulously modeled, with simulations meticulously aligning with particle-in-cell models and Electron Monte Carlo collision simulations. These validations, conducted across both bulk plasma and sheath regions, confirmed the framework's reliability and accuracy.

Furthermore, the framework integrates a machine learning model to evaluate results under various recipe input conditions. This comprehensive approach not only enhances the understanding of plasma behavior but also facilitates the identification of optimal manufacturing conditions. Through meticulous recipe optimization, the framework minimizes undesirable effects such as backside chucking force and variations in thin film thickness, thereby improving overall manufacturing competitiveness and sustainability.

Despite the inherent challenges and limitations, the predictive framework showcased significant potential to revolutionize manufacturing processes in the semiconductor industry. Its high predictive power positions it as a valuable tool for enhancing operational efficiency, driving informed decision-making, and ultimately advancing sustainability goals within the semiconductor manufacturing sector.

Key words
Framework, Semiconductor Fabrication, Plasma simulation, Validation of 300 MM Wafer

I. Introduction

To meet the requirements of Dennard scaling, memory products have been adopting new architectures and process techniques for higher density and performance. As a result, manufacturing costs have increased due to the use of expensive toxic reactant gases or the introduction of EUV technology. Given the nature of memory products, characterized by strong consumables and relatively lower prices compared to chips like ICs and CPUs, reducing manufacturing costs significantly contributes to the profitability of the memory business.

This study proposes an industrial framework for predicting for dechuck step of Pecvd (Plasma enhanced chemical vapor deposition) Fabrication Recipe steps, and aims to evaluate the applicability of simulation and machine learning-based frameworks by comparing and verifying experimental results on 300mm wafers from semiconductor production equipment(Table.1). The recipe is composed of Time, Press(Pressure), Gas1(Gas1 flow rate), Gas2(Gas2 flowrate), Gas3(Gas3 flowrate), Gap(Gap distance), RF Power, and Temp(Temperature) all of which are set by the control program.

Table 1. Conceptual PECVD Fabrication Recipe steps

Condition	Deposition	Plasma	Dechuck	Up
Time[sec]	10	5	5	5
Press[Torr]	2	2	2	0
Gas1[sccm]	7000	7000	7000	3000
Gas2[sccm]	300	0	0	0
Gas3[sccm]	3000	3000	3000	3000
Gap[mm]	8	8	8	50
RF Power[W]	800	400	90	0
Temp[℃]	400	400	400	400

II. Simulation and Validation

A. Theoretical framework for dechucking steps

In PECVD, when plasma is formed, an electrical force occurs between the wafer and the ground electrode, leading to chucking. Semiconductor fabrication utilizes robotic transfer systems to operate factories 365 days a year. If the wafer retains electrical force after plasma processing, the robot cannot move the wafer to its intended position, potentially leading to wafer breakage, misalignment, or triggering alarms

The chucking force per unit area on the wafer backside has been identified through the research of Van Elp, J and Nojiri as primarily influenced by the electron number density (1) [1],[3]. Therefore, to predict the electron number density, a plasma fluid simulation model was employed (2)-(4). Based on the thermo-electric-mechanical formulation and satisfying the first law of thermodynamics(4), a global energy balance was established using the Reynolds Transport Theorem to formulate equations for each species(5)-(9) [4]. Conditions specified in the given equations were considered for each species within the fluid simulation to proceed with the calculations.

$$p = \frac{\varepsilon_0}{2}(V_0 - Re\left(\frac{m_e(jw+\nu)}{e^2 n_e \mu_e}\right) * \frac{l}{A} * i - V_2)^2 * (\frac{\epsilon_4}{\epsilon_4 d_3 + \epsilon_3 d_4})^2 (1)$$

$$\frac{\partial n_e}{\partial t} + \nabla \cdot \Gamma_e = \mathrm{S}\ (2)$$

$$\frac{3}{2}\frac{\partial}{\partial t}(n_e T_e) + \nabla\left(\frac{5}{2}T_e\overrightarrow{\Gamma_e} - X\nabla T_e\right) = P - n_e \sum_r k_r n_r \varepsilon_r\ (3)$$

$$\Gamma_e = -\mu_e n_e \nabla\varphi - D_e \nabla n_e (4)$$

$$\frac{d}{dt}\left(\rho\epsilon + \frac{1}{2}\rho\mathbf{V}\cdot\mathbf{V}\right) + \left(\rho\epsilon + \frac{1}{2}\rho\mathbf{V}\cdot\mathbf{V}\right)\cdot div\boldsymbol{v} + \left\{\varepsilon_0\dot{\mathbf{e}}\cdot\mathbf{e} + \mu_0\dot{\mathbf{h}}\cdot\mathbf{h} + \frac{1}{2}\left(\varepsilon_0\mathbf{e}\cdot\mathbf{e} + \mu_0\mathbf{h}\cdot\mathbf{h}\right)\cdot div\mathbf{v}\right\} = \rho(h_t + \mathrm{f_b}\cdot\mathbf{v}) + \mathrm{r_m}\left(\rho\epsilon + \frac{1}{2}\rho\mathbf{v}\cdot\mathbf{v}\right) + (\mathbf{T_{EM}} + \mathbf{T})\cdot\mathbf{v}\cdot div\mathbf{v} + \frac{d}{dt}(\mathbf{T_{EM}} + \mathbf{T})\cdot\mathbf{v} - div(\boldsymbol{q} + \mathbf{e}\times\mathbf{h})\ (5)$$

$$\rho\dot{\mathbf{v}} = \rho\mathrm{f}_b + div(\mathbf{T_{EM}}) + div(\mathbf{T})\ (6)$$

$$\mathbf{T}\text{-}\mathbf{T}^{\mathbf{T}} = \mathbf{T_{EM}}^{\mathbf{T}} - \mathbf{T_{EM}}\ (7)$$

$$\frac{d\rho}{dt} + div(\rho\mathbf{v}) = \rho\ \mathrm{r_m}\ (8)$$

$$\rho\dot{\boldsymbol{\epsilon}} = \mathbf{T}\cdot grad\mathbf{v} + \rho\ h_t + \rho\ \mathrm{r_m}\epsilon - div(q + \mathbf{e}\times\mathbf{h})\ (9)$$

B. Validation of Bulk plasma in fluid simulation

To validate the results obtained from the fluid model, comparisons were made with a Particle-in-Cell (PIC) analysis of argon plasma, focusing on the spatial distribution of normalized electron number density and electron temperature. The results indicated similar spatial distributions and electron temperature values between the fluid simulation model and the PIC analysis(Fig.1) [2].

Additionally, the trend observed in the PIC paper, where the position of bulk plasma varied with the temperature of the ground electrode, was also confirmed in the results of

the fluid simulation model.

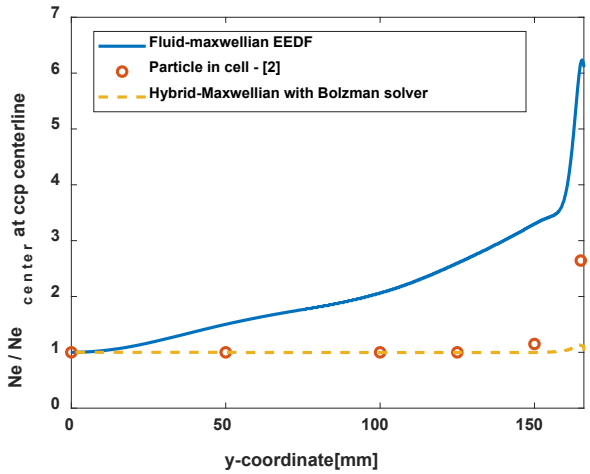

Fig. 1. Normalized electron number density according to wafer radius; Fluid simulation model, Particle in cell(Pic), Hybrid model Validation of ion bombardment via anode sheath

Furthermore, to assess the degree of ion bombardment by argon ions passing through the sheath, the results from the fluid simulation were used as input for an electron Monte Carlo collision simulation to obtain the ion energy distribution function (IEDF) of argon ions (Fig.2) [5]-[7]. When the IEDF values at different distances from the wafer's radius were inputted into the Bohdansky sputtering yield empirical formula, the resulting thickness data were compared with the thickness data measured using optic methods before and after generating argon plasma on a 300mm wafer in semiconductor production equipment (9)-(12) [8],[9] .

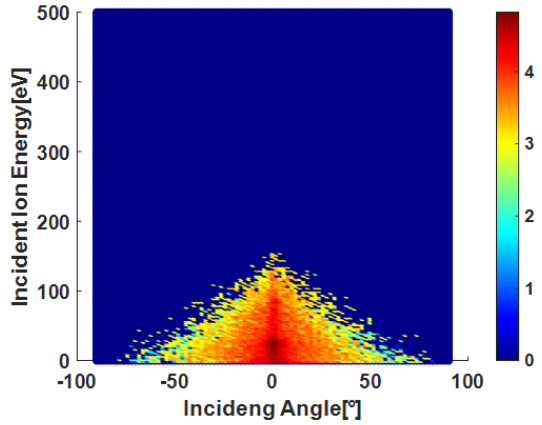

Fig. 2. Calculated Iedf(Ion energy distribution function) at each point on wafer frontside

We used Pecvd to form silicon oxy nitride at 800 angstroms (Fig.3) and silicon dioxide at 1000 angstroms, then compared the thin film thickness before and after exposure to argon plasma using optical measurements to assess the thickness of the film that was ejected.

The comparison showed a similar spatial distribution trend between the two sets of data which one data is predicted sputtering yield by impirical formula and simulation, the other is removed film thickness measured by optic measurement equipment.

$$Y = (6.4 * 10^{-3}) * m_r * \gamma^{\frac{5}{3}} * E^{0.25}\left[1 - \frac{E_{th}}{E}\right]^{3.5} \quad (9)$$

$$\gamma = \frac{4m_r m_p}{(m_r + m_p)^2} \quad (10)$$

$$\frac{m_p}{m_r} > 0.3 \quad (11)$$

$$E_{th} = 8 * U_{sb} * \left[\frac{m_p}{m_r}\right]^{\frac{2}{5}} \quad (12)$$

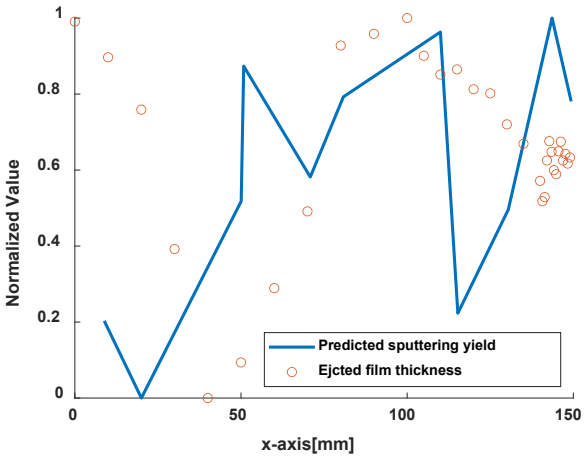

Fig. 3. Normalized optic measurement of ejected SiO_xN_y film by argon plasma and predicted sputtering yield Trained Machine Learning Regression model

The fluid simulation was conducted for 55 cases varying temperature, pressure, Ccp gap distance between electrodes, and argon flow rate for a specific geometry. Raw data from these simulations were used to select a Gaussian process regression(GPR) model that best mimicked the simulation results(Table.2). The chosen machine learning model was then utilized to predict recipe conditions within a window.

Table 2. Performance of trained machine learning regression models

Model	Linear	Ensemble	Svm	Tree	GPR
Method	Interaction	Bagged	Fine gaussian	Fine	Rational quadratic
RMSE	3.12	0.69	0.87	0.73	0.60
R^2	0.34	0.97	0.95	0.97	0.98
MSE	10.24	0.47	0.76	0.53	0.36
MAE	2.31	0.23	0.44	0.27	0.17
SPEED	~140000	~76000	~46000	~150000	~5100

C. framework based machine learning and statistical analysis

To minimize the impact on the wafer's front side, the goal was to find conditions where the electron number density

was uniform at the center and edge of the wafer. An ANOVA analysis was performed on the electron number density grouped by the wafer's position (center, mid, edge), selecting conditions where the error between each spatial point's electron number density within groups was minimized. This approach allowed the framework to find conditions that ensured uniformity at the center and edge of the wafer's front side.

Simultaneously, conditions were sought to minimize backside chucking force. Conditions were selected based on ANOVA results, sorting them in ascending order and choosing the conditions with the lowest average value. These framework-derived recipe conditions were then tested by inserting 300mm wafers into memory production equipment and re-measuring the results using optic methods.

The results from testing the recipe conditions identified by the framework aligned closely with the simulation results, with minimal ANOVA errors and backside chucking force. However, for the backside, testing was challenging due to the narrow area after wafer processing, making it difficult to discern differences through Rq results. Therefore, ongoing experiments aim to form a film other than natural oxide on the backside for comparison.

III. Conclusion

This study utilized plasma simulation and machine learning to evaluate the feasibility of simulating a specific step in the pecvd recipe within semiconductor fabrication processes. Given the characteristics of the cvd process, which primarily uses plasma and mixed gases at intermediate pressures, a fluid simulation model suitable for subsequent research was employed. This model was compared with the Particle in cell method, a technique within plasma simulation.

Additionally, the ion energy distribution function (IEDF) of argon ions was determined using fluid simulation and electron Monte Carlo collision simulation. The results, when applied to an empirical formula, showed consistency with experimental measurements of film thickness on wafers before and after deposition in actual equipment.

This research experimentally confirmed the potential of using simulation and machine learning models for predicting semiconductor processes and improving fabrication recipes.

In our future work, we will conduct experimental verifications focusing on species like oxygen that produce negative ions, pivotal for refining the PECVD process. Building on these findings, we aim to broaden our investigation to plasma processes involving a mixture of species, reflective of real semiconductor manufacturing settings. Moreover, our research will extend beyond the plasma generation chamber to include the entire system, such as the matching network. This approach is designed to enhance our ability to manage and improve the PECVD process, optimizing it for more efficient manufacturing, fabrication, and mass production. Our ultimate goal is to develop an integrated framework that enhances process control and increases production scalability across the entire suite of equipment.

Acknowledgment

This work was supported by the Memory CVD Technology Team at Samsung Electronics, the National Research Foundation of Korea (NRF) grant (No. 2022R1A4A1031182), and the Technology Innovation Program (Public-private joint investment semiconductor R&D program (K-CHIPS) to foster high-quality human resources) (RS-2023-00236091, Hybrid bonding technologies for 3D package interconnects) funded by the Ministry of Trade, Industry & Energy (MOTIE, Korea).

References

[1] VAN ELP, J.; GIESEN, P. T. M.; DE GROOF, A. M. M. Low-thermal expansion electrostatic chuck materials and clamp mechanisms in vacuum and air. Microelectronic engineering, 2004, 73: 941-947.

[2] PARK, Geonwoo, et al. Kinetic Analysis of Electrode Heating Effects in a Torr-Regime Capacitively Coupled Plasma Reactor: 2-D Particle-in-Cell Simulation Study. IEEE Transactions on Plasma Science, 2022, 50.2: 540-549.

[3] Kazuo Nojiri, " Dry Etching Technology for Semiconductors", Springer International Publishing, 67-70p

[4] SIM, Jin-Woo, et al. Effective thermo-electric-mechanical modeling of capacitively coupled plasma in low-pressure conditions: Modeling and application in dry etching. Applied Mathematical Modelling, 2024, 127: 32-59.

[5] KUSHNER, Mark J. Monte-Carlo simulation of electron properties in rf parallel plate capacitively coupled discharges. Journal of applied physics, 1983, 54.9: 4958-4965.

[6] KUSHNER, Mark J. Hybrid modelling of low temperature plasmas for fundamental investigations and equipment design. Journal of Physics D: Applied Physics, 2009, 42.19: 194013.

[7] KUSHNER, Mark J., et al. DOE Plasma Science Center-Predictive Control of Plasma Kinetics: Multi-Phase and Bounded Systems (Final Report DE-SC0001939). Univ. of Michigan, Ann Arbor, MI

[8] BOHDANSKY, J. A universal relation for the sputtering yield of monatomic solids at normal ion incidence. Nuclear Instruments and Methods in Physics Research Section B: Beam Interactions with Materials and Atoms, 1984, 2.1-3: 587-591

[9] Garcia-Rosales, C., W. Eckstein, and J. Roth. "Revised formulae for sputtering data." Journal of nuclear materials 218.1 (1995): 8-17.